Supporting Information

Structural Basis for DNA Gyrase Interaction with Coumermycin A1

*Arnaud Vanden Broeck, Alastair G. McEwen, Yassmine Chebaro, Noëlle Potier, Valérie Lamour**

TABLE OF CONTENT

EXPERIMENTAL SECTION

Protein Expression and Purification. The sequences coding for the *Escherichia coli* (*Ec*) and *Thermus thermophilus* HB8 (*Tth*) GyrB 43K fragments (Supporting Information Figure S1a) (residues M1 to R393 or V390, respectively) were inserted between the *NdeI* and *BamHI* restriction sites of a pET28a derived vector containing an N-terminal 10 His-tag. Overexpression was performed in *E. coli* BL21 (DE3) in LB medium containing 50 mg/L kanamycin. Cells were induced with 0.4 mM IPTG after reaching an OD_{600} 0.8–0.9 and proteins were expressed at 37°C for 3 h. Cells were harvested and resuspended in lysis buffer (20 mM Hepes, 500 mM NaCl, 10 mM imidazole, 5% v/v glycerol, pH 8.0) and lysed with 3 cycles of high-pressure disruption using EmulsiFlex-C3 at 1500 bars. Both GyrB 43K fragments from *E. coli* and *T. thermophilus* were first purified by nickel-affinity chromatography on a manually packed XK 26/20 column (Pharmacia) with Chelating Sepharose 6 Fast Flow resin (GE healthcare) bound to Ni^{2+} ions. Elution was performed with the lysis buffer containing 250 mM imidazole pH 8.0. The His-tag was subsequently cleaved by PreScission protease (P3C) cleavage (mass ratio 1:50 43K-P3C) overnight at 4°C in a dialysis buffer A (10 mM Tris-HCl, 60 mM NaCl, 1 mM EDTA, 1 mM DTT, 5% v/v glycerol, pH 8.0). Proteins were then further purified by an anion exchange chromatography step using a HiTrap Q HP column (GE Healthcare). The protein was eluted with a linear gradient of 20 column volumes with buffer B (10 mM Tris-HCl, 1M NaCl, 1 mM EDTA, 1 mM DTT, 5% v/v glycerol, pH 8.0). Fractions containing GyrB 43K were pooled and loaded on a Superdex S200 16/60 size-exclusion chromatography column (GE Healthcare) using 50 mM Tris-HCl, 125 mM NaCl, 1 mM EDTA, 1 mM DTT, 5% v/v glycerol, pH 8.0. After the purification process, 180 mg of GyrB 43K were obtained from 3 L of cultures for both species (Figure S1b). GyrB 43K fractions (3-4 mg/ml) were flash-frozen in liquid nitrogen for storage at -80°C.

GyrB 43K-COU Co-crystallization Experiments. The *Ec* 43K-COU crystals grew at 20°C in 0.2 mM NaH2PO4, 22% (v/v) PEG 3350, pH 8.0 and the *Tth* complex crystals grew at 20°C in 100 mM imidazole pH 7.0, 48% (v/v) 2-Methyl-2,4-pentanediol (MPD).

Crystallographic Data Collection, Structure Determination and Refinement. Data were collected at the PROXIMA-1 beamline (SOLEIL, Gif-sur-Yvette, France) and the ID30b beamline (ESRF, Grenoble, France). Diffraction data were processed using XDS [1]. The structure of the *Ec* and *Tth* GyrB 43K-COU complexes were determined by molecular replacement with PHASER [2] using PDB entries 1EI1 [3] and 1KIJ [4] as models, respectively. COU constraints dictionary was generated using the GRADE server from Global Phasing (http://grade.globalphasing.org) using a MOL2 file generated using MarvinSketch (ChemAxon). Initial models were manually improved in COOT [5] and followed by iterative refinement with BUSTER [6]. Figures were created with PyMOL (Schrödinger, LLC) and UCSF ChimeraX, developed by the Resource for Biocomputing, Visualization, and Informatics at the University of California, San Francisco [7].

Native Mass Spectrometry. 50 µM of both *Ec* and *Tth* GyrB 43K subunits were mixed with 75 µM COU in the last purification buffer. The buffer of the GyrB 43K-coumermycin complexes were exchanged with 200 mM ammonium acetate at pH 7.5 using mini gel filtration columns (Microbiospin 6, Biorad). Native electrospray ionization mass spectrometry ESI-MS measurements were performed on an electrospray

time-of-flight mass spectrometer (MicrOTOF, Bruker Daltonic, Germany). The capillary exit voltage was set to optimize the desolvation process while preventing dissociation of the non-covalent species (300–400V). Samples were diluted to 20 µM in the same buffer and continuously infused into the ESI ion source at a flow rate of 3 µL/min through a Harvard syringe pump (Harvard Apparatus model 11).

Analytical Size-exclusion Chromatography. Analytical size-exclusion chromatography with the *Ec* and *Tth* GyrB 43K, GyrB, GyrA subunits and DNA Gyrase ($GyrA_2B_2$) in the presence or absence of COU (Sigma) (molar ratio 1:1.5 43K-COU) were performed with a Superdex S200 10/300GL (GE Healthcare) in 50 mM Tris, 125 mM NaCl, 1 mM EDTA, 1 mM DTT, 5% v/v glycerol, pH 8.0. Approximate molecular weights were calculated based on a calibration curve obtained with the Gel Filtration Standard kit (Biorad 151-1901), run on the same column in the same buffer.

SAXS Experiments. Small Angle X-ray Scattering (SAXS) data of both *Ec* and *Tth* GyrB 43K-COU complexes were collected at the BM29 BioSAXS beamline (ESRF, Grenoble, France), equipped with a Pilatus 1M detector (distance to sample 2.867 m) and an on-line size exclusion chromatography system. The energy of the X-ray beam was 12.5 keV (wavelength λ = 0.9919 Å) and the setup adjusted to achieve scattering q values of $0.0057 < q < 0.493$ Å^{-1} ($q = 4\pi \sin(\theta)/\lambda$, where 2θ is the scattering angle). The experiments were carried out at room temperature with the injection of 100 µl of the complexes at 20 mg/ml in a S200 10/300 Increase column equilibrated with 20 mM Tris, 125 mM NaCl, 0.5 mM TCEP, 5 mM DTT, 2% v/v glycerol, pH 8.0 and directly coupled to a tight quartz capillary exposed to the X-ray beam. Samples were injected at 0.8 ml/min for 30 min and frames of 2 sec were recorded during the whole run. All the data processing steps were performed using the program package PRIMUS [8]. The radius of gyration (R_g) was computed using the Guinier approximation assuming that at very small angles ($q < 0.01$ Å^{-1}) the intensity is represented as $I(q) = I(0)\exp(-(qRg)^{2/3})$ [9]. The distance distribution function ($P_{(r)}$) and the maximal particle dimension (D_{max}) were calculated with the indirect transform package GNOM [10]. Low resolution shapes of the complexes were computed by the program DAMMIF [11] considering low angle data ($q < 8/Rg$ Å^{-1}) using a 2-fold axis symmetry. Each DAMMIF model showed good fit to the experimental SAXS curve ($\chi^2 = 0.8$~1.0).

***Ab Initio* Calculations.** The structures of the COU molecule were optimized by *ab initio* calculations using the software Gaussian 09 [12]. Geometry optimization of the different COU conformations was performed using the Hartree-Fock method with the 6-31G* basis set (HF/6-31G*) until convergence was reached and respective energy minima obtained for each starting point. To create new *trans* and *cis*-isomers of COU, one carbonyl group of each respective structure of COU from *Ec* and *Tth* complexes were flipped using the program COOT. We observed that the carbonyl groups around the central pyrrole were likely to form hydrogen bonds with hydroxyl groups located on the aminocoumarin rings. To assess whether these interactions determine the conformation of the aminocoumarin rings, the carbonyl groups were flipped in silico from a *trans* to a *cis* position in the COU from the *Ec* structure while maintaining the rest of the molecule fixed. After *ab initio* calculations, the lowest energy conformation obtained showed that the aminocoumarin ring, the deoxy-L-noviose and the pyrrole substitutes recover a similar conformation as in the *Tth* structure where the carbonyls are *cis* (Figure S8c). This result shows that the hydrogen bond between the carbonyls and the hydroxyl is recovered, forcing the whole extended arm to move. Similar calculations were also performed from a

starting structure identical to the one in the *Tth* complex where the carbonyl moieties are changed from a *cis* to *trans* conformation and similar results were obtained (Figure S8d).

Protein Surface Analysis. The protein surface analysis was performed using the PISA (Protein interfaces, surfaces and assemblies) server (EMBL-EBI). Solvation energy for each were calculated, as well as the gain percentage on complex formation and the P-value indicating if the interface is due to crystal packing (P-value>0.5) or if it is biologically relevant (P-value<0.5) [13].

Thermal Denaturation Assay Thermal denaturation analysis of the *Ec* and *Tth* GyrB 43K subunits were performed by DSF (Differential Scanning Fluorimetry) in the presence or absence of COU using the Prometheus NT.48 apparatus (NanoTemper Technologies). For the complex formation, 50 µM of the GyrB 43K subunits were incubated with 75 µM of COU in 50 mM Tris-HCl, 125 mM NaCl, 1 mM EDTA, 1 mM DTT, pH 8.0. The intrinsical fluorescence signal was detected during a temperature gradient between 20°C to 95°C at a rate of 1°C/min. First derivative of the sigmoid curves provides fusion temperatures (T_m) of the proteins, corresponding to the denaturation midpoint.

SUPPLEMENTAL TABLES

	***E. coli* 43K-COU**	***T. thermophilus* 43K-COU**
	PDB 6ENG	**PDB 6ENH**
Data collection		
Resolution range (Å) [a]	33.31-2.3 (2.382-2.3)	22.94-1.94 (2.009-1.94)
Space group	$P2_12_12_1$	C2
Cell dimensions		
a, b, c (Å)	47.83 128.07 159.76	166.37 37.85 66.75
α, β, γ (°)	90 90 90	90 110.24 90
Unique reflections	43590 (3696)	28207 (2857)
Multiplicity	6.3 (5.1)	2.7 (2.7)
Completeness (%)	97.41 (83.52)	95.89 (97.73)
R-Merge [b]	0.1261 (1.457)	0.01998 (0.9675)
R-Meas [b]	0.02462 (1.199)	0.1378 (1.625)
$CC_{1/2}$ [c]	0.998 (0.604)	1 (0.554)
CC* [c]	0.999 (0.868)	1 (0.844)
Mean I/σ(I) [b,c]	9.89 (0.83)	18.95 (0.86)
Refinement		
Reflections	43470 (3689)	28173 (2844)
Resolution (Å)	2.3	1.94
R-work [d]	0.2082	0.2007
R-free [d]	0.2662	0.2405
No. atoms for protein/ligands/solvent	5893/124/390	2829/90/90
Protein residues	750	366
Rmsd bonds/ angle (Å/°)	0.014/1.81	0.014/1.62
Ramachandran statistics (%) [b,e]	96.91/2.69/0.40	98.06/1.67/0.28
Clash score	1.85	2.94
Average B ($Å^2$)	65.03	79.56

Table S1. Data collection and refinement statistics.

a: Values in parentheses correspond to the highest-resolution shell.

b: Calculated with Phenix [14] "phenix.table_one".

c: Correlation coefficient between two randomly chosen halves of the data set [15]. The quality of the data was monitored based on $CC_{1/2}$ and CC* metrics.

d: R_{free} was calculated as R_{work} using the 5% of reflections that were selected randomly and omitted from refinement [16].

e: Percentage of amino acid residues in the favored, allowed, and disallowed regions, respectively.

	Ec 43K	***Ec 43K-COU****	***Tth 43K***	***Tth 43K-COU****
Exclusion Chromatography				
Elution volume (ml)	15.29	13.53	15.14	14.36
Estimated molecular weight (kDa)	44.25	93.29	47.35	66.15
Native Mass Spectrometry				
Molecular weight (Da)	43,676 ±1	88,460 ±1[£]	42,938 ±2	86,993 ±4[$]
Thermal Denaturation Assay				
Fusion temperature Tm (°C)	51.8	53.9	88.4	90.1
∆T (°C)		+2.1		+1.7
SAXS Experiments				
R_g (Guinier Approximation) (nm)	2.61	3.58	2.61	3.36
Real-space R_g ($P_{(r)}$) (nm)	2.66	3.64	2.68	3.40
Dmax (nm)	9.14	12.30	9.15	15.10

Table S2. Biophysical characterization of the 43K-COU complexes from *E. coli* and *T. thermophilus*.

***** COU molecular weight is 1110 Da.

[£] Two *Ec* 43K subunits (43,676 Da + 43,676 Da) plus one COU molecule (1110 Da) = 88,462 Da

[$] Two *Tth* 43K subunits (42,938 Da + 42,938 Da) plus one COU molecule (1110 Da) = 86,986 Da

	E. coli				*T. thermophilus*			
PDB ID	6ENG				6ENH			
Selection range	Chain A		Chain B		Chain A		Chain A sym	
Residues implicated in interface	G81, I82, P84		G81, I82, P84		Y52, R73, E134, R159, G160		Y52, R73, E134, R159, G160	
Number of residues								
Interface	3	0.8%	3	0.8%	5	1.4%	5	1.4%
Surface	341	89.7%	341	90.7%	335	91.5%	335	91.5%
Total	380	100.0%	376	100.0%	366	100.0%	366	100.0%
Solvent-accessible area, Å²								
Interface	69.2	0.3%	69.2	0.3%	131.1	0.7%	131.1	0.7%
Total	18074.8	100.0%	18351.8	100.0%	18408.0	100.0%	18408.0	100.0%
Solvation energy, kcal/mol								
Isolated structure	-339.3	100.0%	-339.3	100.0%	-337.9	100.0%	-337.9	100.0%
Gain on complex formation	-1.1	0.3%	-1.1	0.3%	-0.9	0.3%	-0.9	0.3%
P-value*	0.323		0.323		0.314		0.314	

Table S3. Surface interface analysis using the PISA server.

* P-value lower than 0.5 represents a specific interaction of residues at the surface interface [13].

SUPPLEMENTAL FIGURES

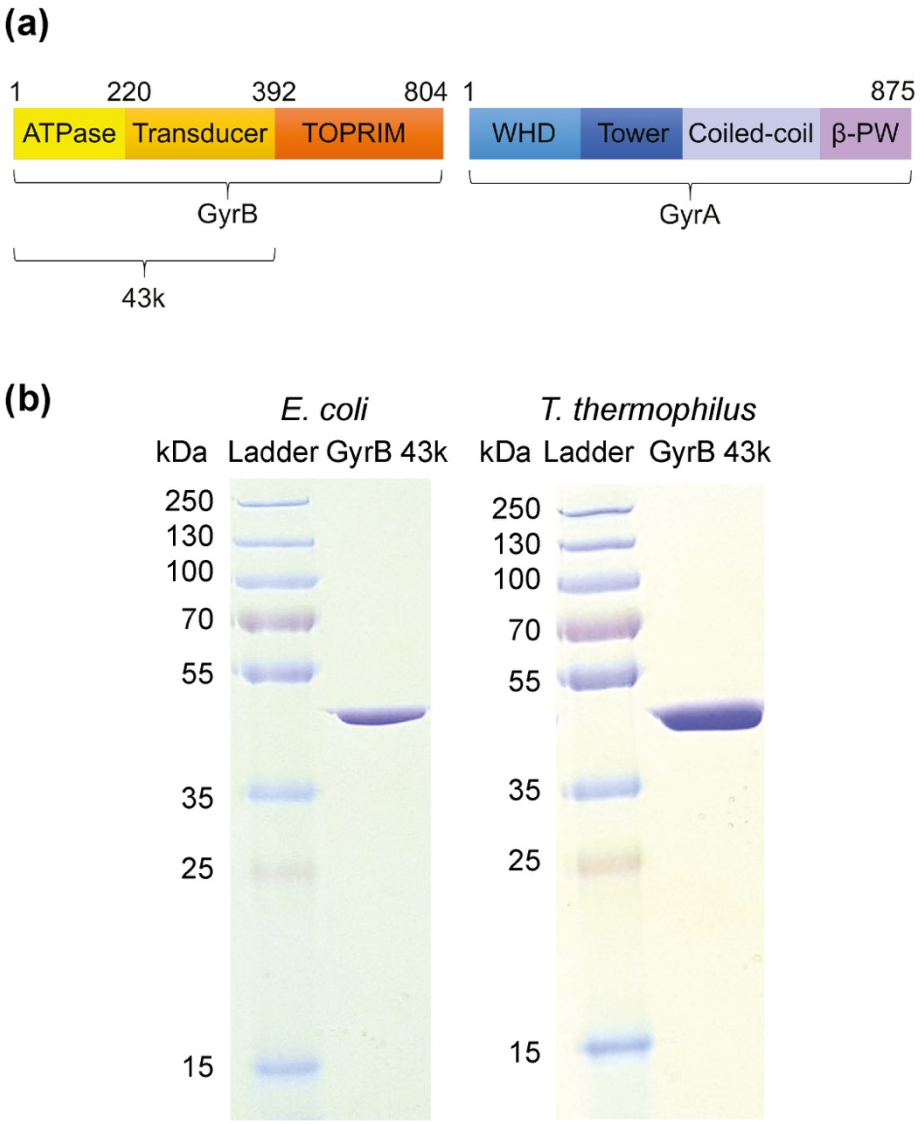

Figure S1. DNA Gyrase and GyrB 43K domain protein samples analysis. **(a)** Primary structures of the *E. coli* GyrB and GyrA subunits. 43K fragment includes the GHKL ATPase and Transducer domains. (**b**) SDS-PAGE analysis of the *E. coli* and *T.thermophilus* 43K proteins after 3 purification steps.

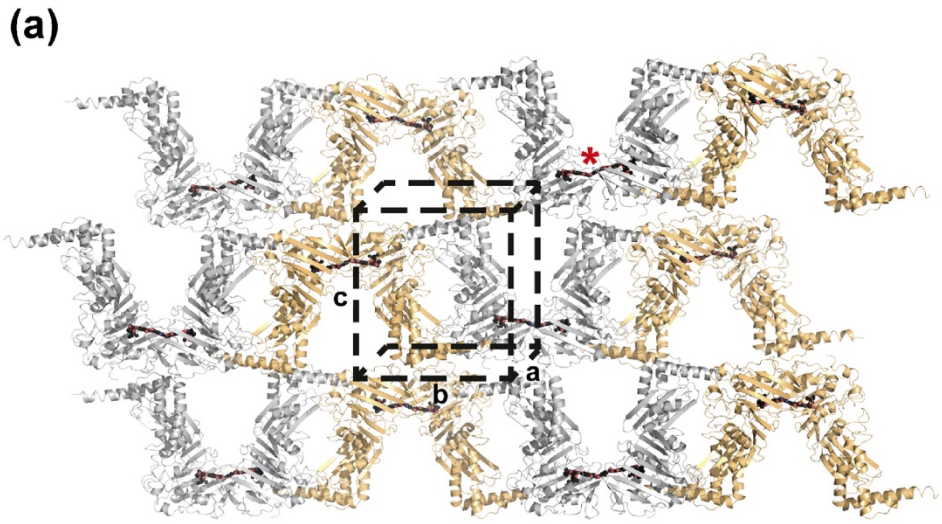

$P2_12_12_1$

a, b, c (Å)	47.87, 128.19, 159.87
α, β, γ (°)	90, 90, 90

* coumermycin-A1

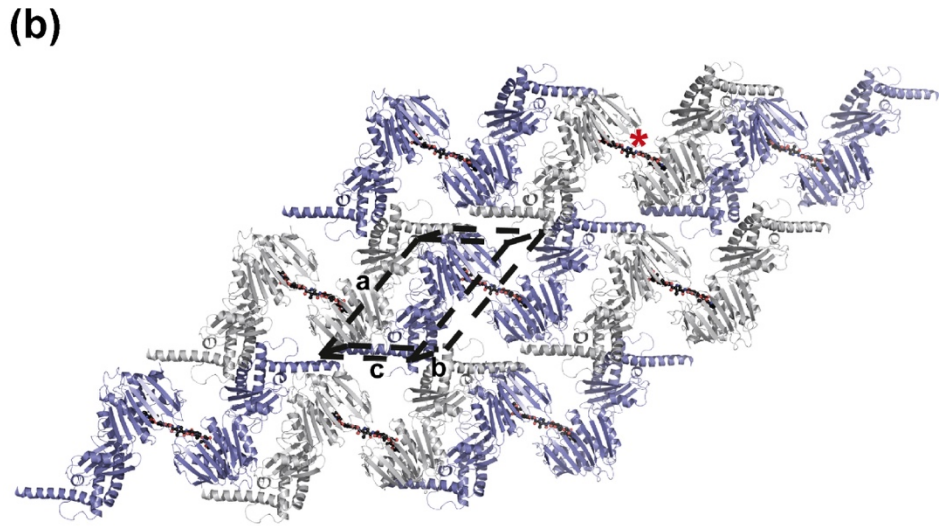

C2

a, b, c (Å)	166.37, 37.85, 66.75
α, β, γ (°)	90, 110.24, 90

* coumermycin-A1

Figure S2. Crystal packing of the 43K-COU complexes. **(a)** Crystal packing of the *E. coli* 43K-COU complex. **(b)** Crystal packing of the *T. thermophilus* 43K-COU complex. Dashed lines represent the asymmetric unit. Coumermycin A1 is highlighted by a red asterisk.

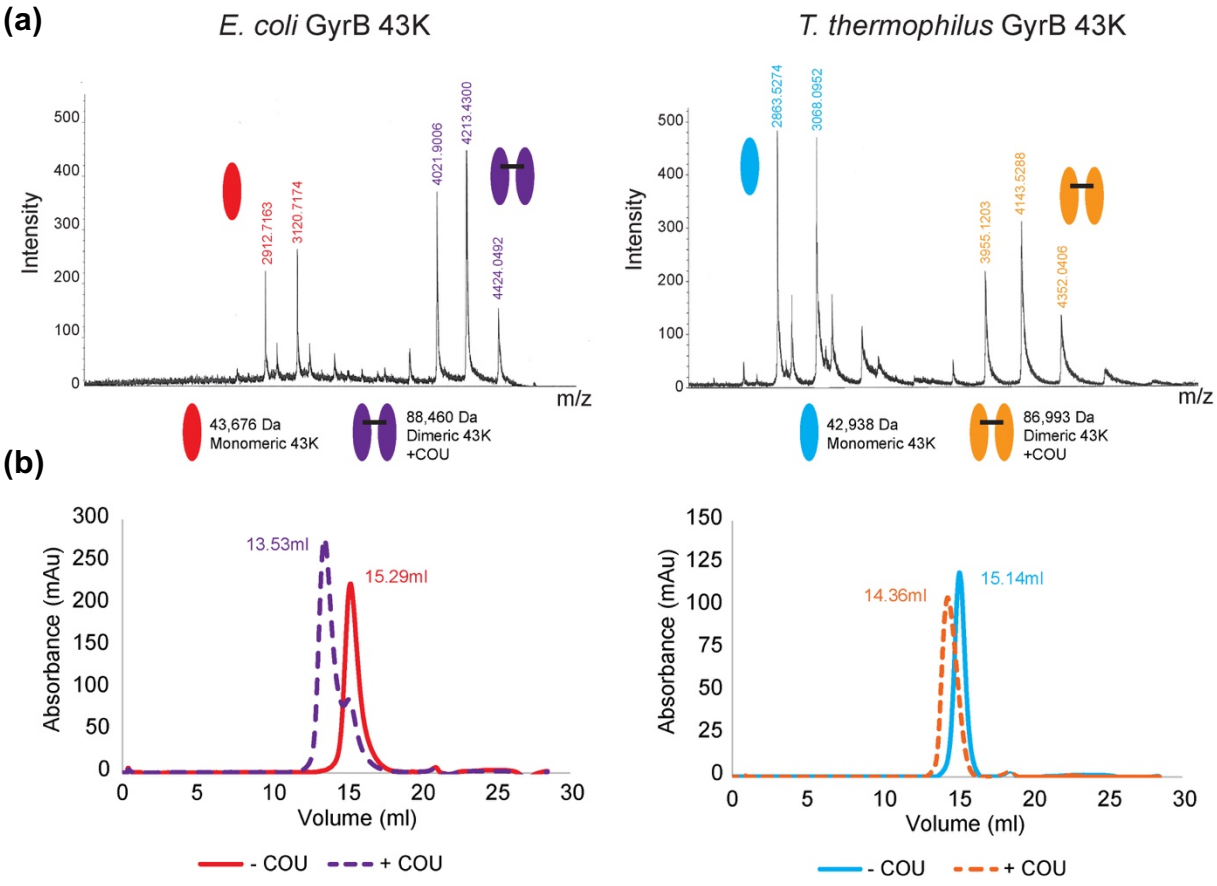

Figure S3. **In solution biophysical characterization of the GyrB 43K-COU complexes**. **(a)** Native mass spectrometry analysis of *E. coli* (left) and *T. thermophilus* (right) GyrB 43K in complex with COU. Each complex in presence or absence of COU has a particular mass and exists under multiple charges states. The shift of the mass spectra to higher m/z witnesses the formation of a stable complex of GyrB 43K with COU. Attribution of the m/z peaks allows to calculate the precise mass of each complex. Ovals represent a GyrB 43K monomer and the black line represents COU. Ovals are colored based on the complex colors used in (b). The measured masses and stoichiometry are indicated under each complex peaks'. The experiment confirms that COU traps 2 monomers, with minor population of free or liganded monomers appearing at higher column voltage. **(b)** Size-exclusion chromatography of *E. coli* (left) and *T. thermophilus* (right) GyrB 43K alone or in complex with COU. Size exclusion chromatograms are colored in red for *E. coli* GyrB 43K in absence of COU, dashed purple for *E. coli* GyrB 43K in presence of COU, blue for *T. thermophilus* GyrB 43K in absence of COU and dashed orange *for T. thermophilus* GyrB 43K in presence of COU.

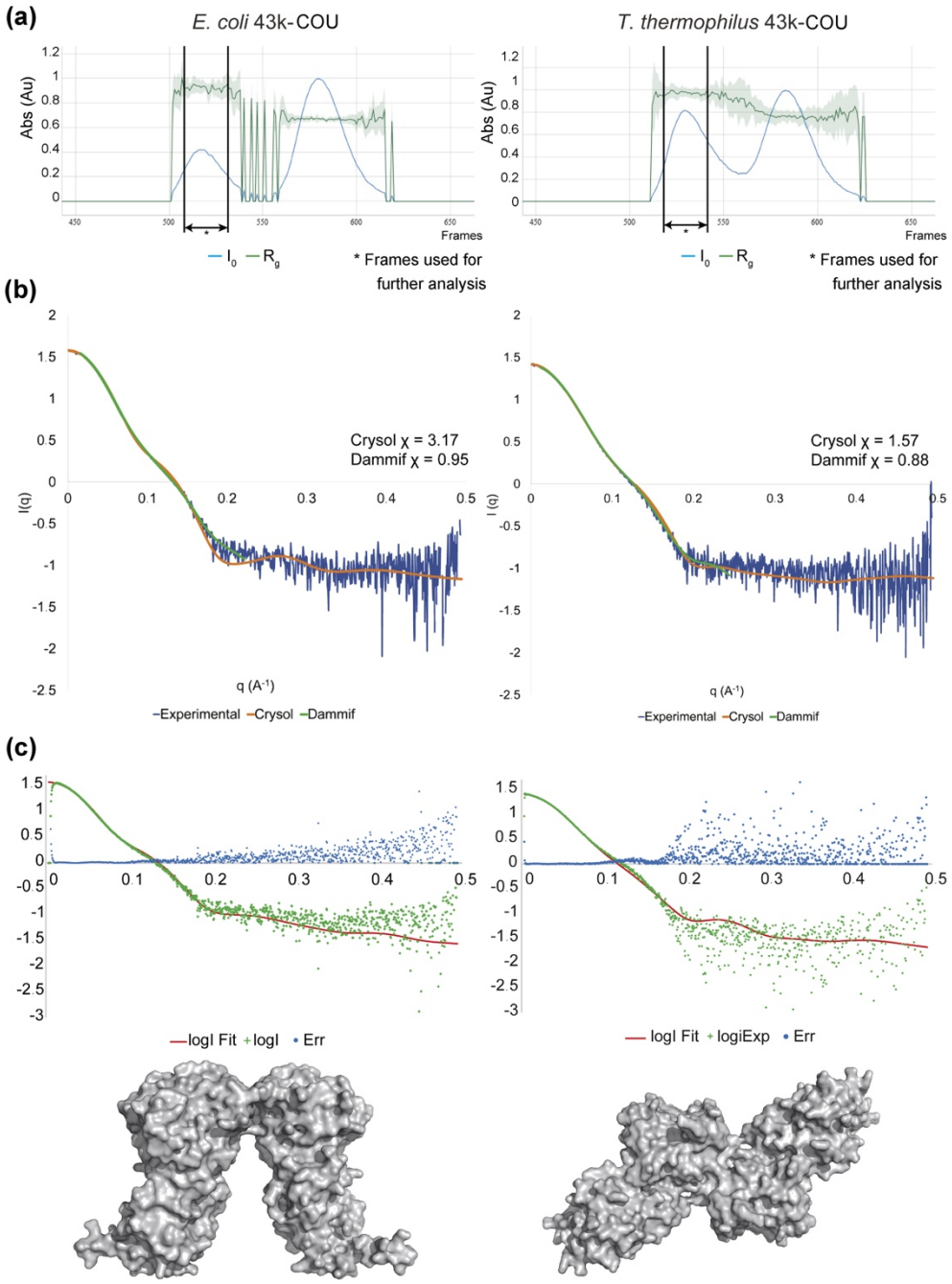

Figure S4. Raw SAXS data and validation experiments. Results are shown for *E. coli* (left) and *T. thermophilus* (right) 43K-COU complexes. **(a)** SEC-SAXS chromatogram showing gel filtration elution peaks (blue) and corresponding R_g values (green). Frames corresponding to the buffer before the elution peak were used to generate background scattering curves. R_g values were measured during the run to follow the change in size of the samples, allowing one to select frames corresponding to monodisperse populations. **(b)** Experimental $Ln(I_{(q)})$ curves with the *ab-initio* DAMMIF curve fit (green) using the Damstart (DAMAVER) as an initial constraint and the CRYSOL [17] fit (orange) of the X-ray structures. **(c)** Rigid-body modelling of the 43K-COU complexes using the atomic models in monomeric form of *E. coli* (PDB ID: 1EI1 chain A) and *T. thermophilus* 43K (PDB ID: 1KIJ chain A) with the SASREF package [18] During the process, the distance between the 2 monomers was forced to reproduce the spacing imposed by the COU itself in the structures. Green dots represent the experimental $Ln(I_{(q)})$ data, the red curve is the fit of the calculated rigid-body models (grey volumes under the curves) with respect to the experimental curve and blue dots correspond to the error of the fit.

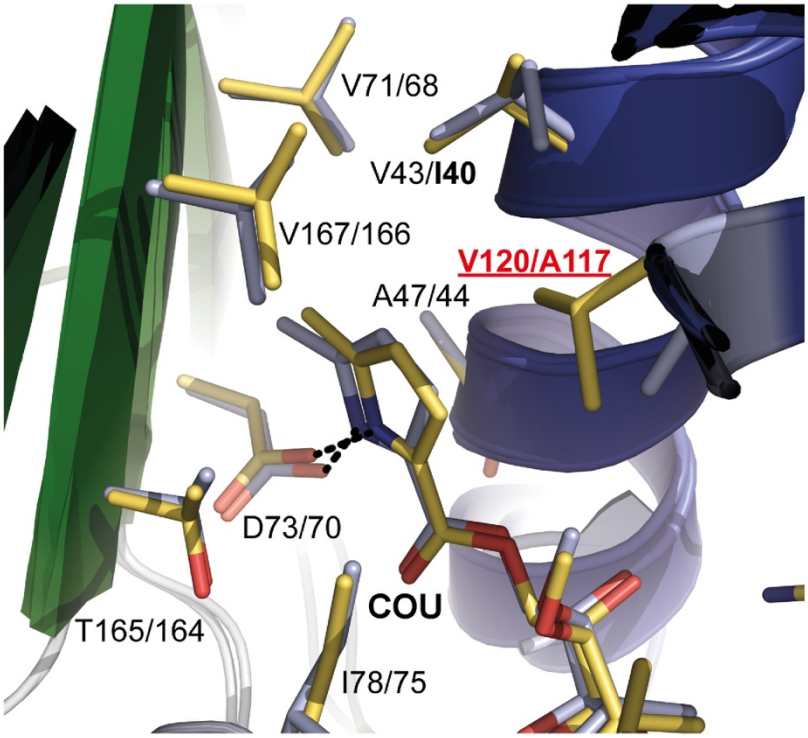

Figure S5. Superimposition of the binding sites of *E. coli* and *T. thermophilus* 43K-COU around the terminal pyrrole. In *E.coli* **(a),** Val120 participates to the hydrophobic interaction with COU while its counterpart in *T. thermophilus*, Ala117, does not. Likewise, Gly101, Phe104 and Asp105 in *E. coli* are part of the ATP lid and stabilize COU by hydrophobic contacts.

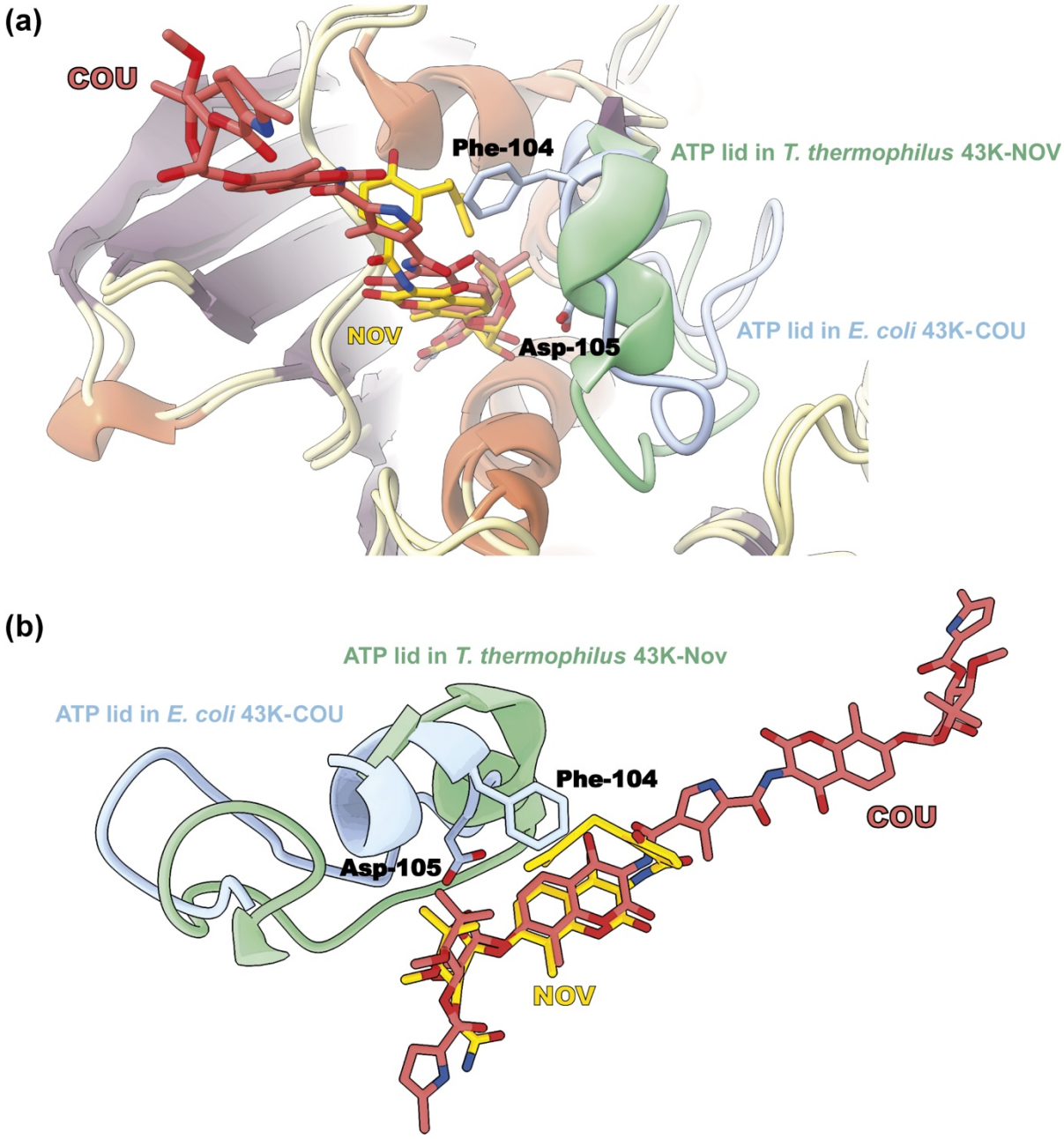

Figure S6. Comparison of ATP lid position in the *E. coli* 43K-COU and the *T. Thermophilus* 43K-NOV structures. **(a)** View of the ATPase pocket with both ATP lids on the right side. ATP lid from *E. coli* 43K-COU structure (PDB ID 6ENG) is colored in pale blue and the one from *T. thermophilus* 43K-NOV structure (PDB ID 1KIJ) is colored in pale green. **(b)** Different view of the superimposition with ATP lids only.

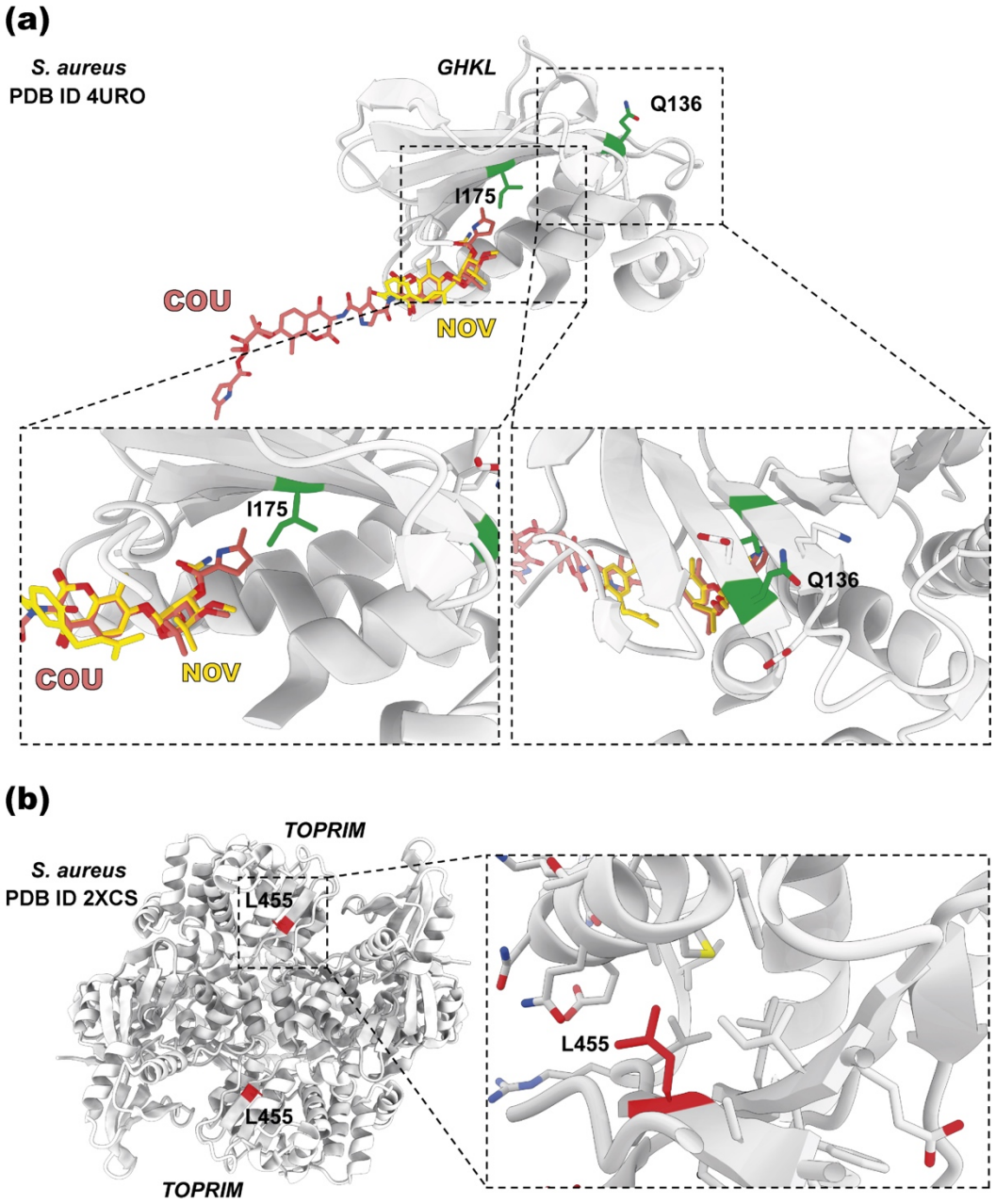

Figure S7. Structural analysis of a *S. aureus* coumermycin A1 resistant gyrase. **(a)** The *S. aureus* GyrB 24K-Novobiocin (PDB ID 4URO) structure was used to map the residues I175 and Q136 found in the coumermycin A1 resistant strain. Our structure of *Ec* GyrB 43K-COU was aligned with respect to the 20-220 residues of the *S. aureus* GyrB 24K in order to visualize the coumermycin A1 position in the *S. aureus* GyrB 24K structure. Residue I175 is found in the vicinity of the terminal pyrrole of coumermycin A1. The mutation I175E changes the polarity in the binding pocket, conferring an unfavorable interaction and resistance to coumermycin A1. Residue Q136 is present at the surface of the GHKL domain and seems involved in the stabilization of secondary structure elements constituting the GHKL domain. Mutation of this residue into glutamic acid might impair allosteric movements between GHKL and transducer domains and could increase resistance to coumermycin A1. **(b)** Residue L455 is part of a hydrophobic patch in the TOPRIM domain of GyrB in *S. aureus* cleavage complex structure (PDB ID 2XCS). Its mutation into isoleucine might also impair allosteric movements by rigidifying the hydrophobic interactions in the vicinity, leading to decreased activity and coumermycin A1 resistance.

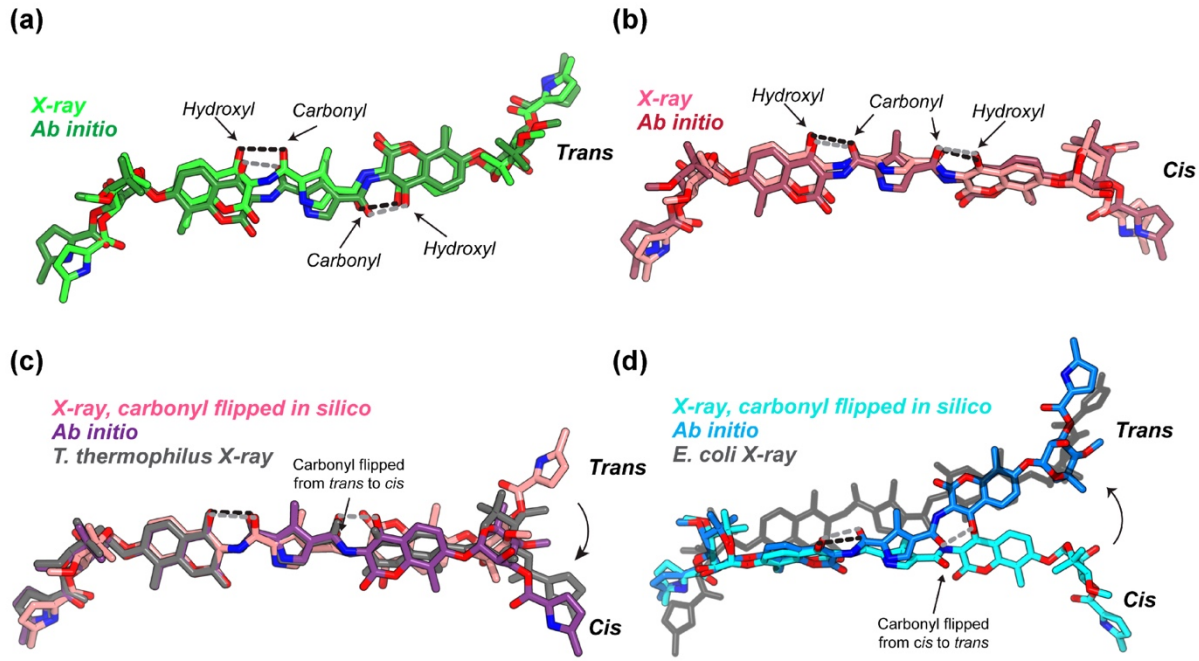

Figure S8. Geometry optimization for the COU molecules. Starting conformations of the COU from *E. coli* (**a**) and *T. thermophilus* (**b**) structures are represented in light green and pink respectively, *ab initio* energy minima from each starting point are superimposed on the initial structure and colored in dark green and dark pink respectively. Hydrogen bonds between the carbonyl and the hydroxyl from the aminocoumarin ring are represented in dashed lines: black for the starting conformation, grey for the geometry optimized conformation. **(c)** The generated starting structure of a cis-isomer of COU from the *E. coli* structure (carbonyl flipped from *trans* to *cis*) is shown in pink, and the corresponding *ab initio* energy minimum in purple, with the structure of COU from *T. thermophilus* in transparent black for comparison. **(d)** Similarly, the generated trans-isomer of COU from the *T. thermophilus* structure (carbonyl flipped from *cis* to *trans*) is shown in cyan and the corresponding ab initio minimum in blue, with the structure of COU from *E. coli* in transparent black for comparison. In brief, no alternative conformations were found during the geometry optimizations that was performed, suggesting that these two isomer structures are the most two stable energy minima. Moreover, the two isomeric forms are stabilized by the hydrogen bonds between the carbonyls surrounding the central pyrrole and the hydroxyl groups situated on the aminocoumarin rings.

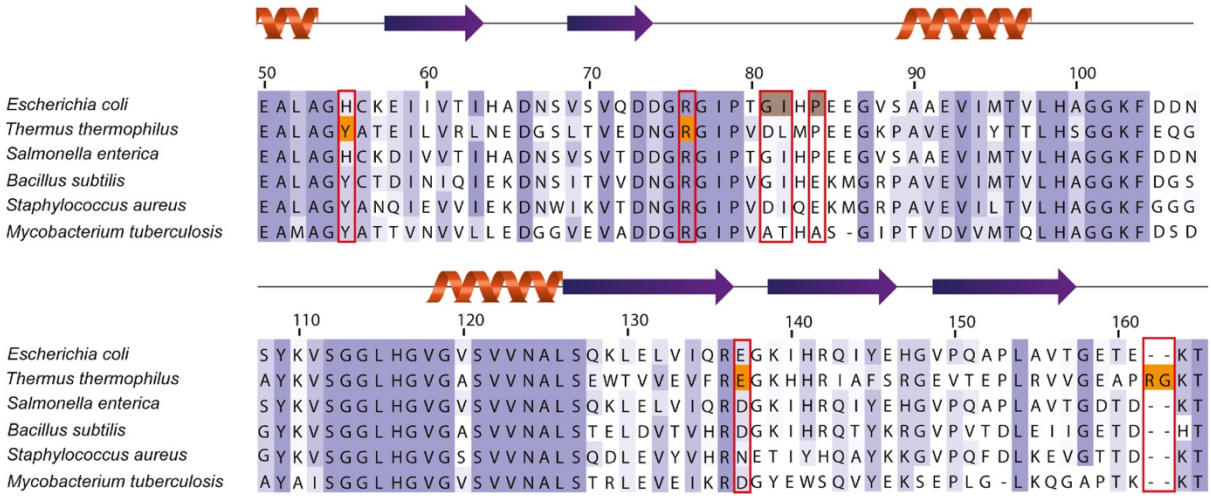

Figure S9. Multiple sequence alignment for the dimer interface region. Multiple alignment performed with COLBAT (NCBI) of GyrB 43K from 3 gram negative bacteria (*Escherichia coli, Thermus thermophilus, Salmonella enterica*) and 3 gram positive bacteria (*Bacillus subtilis, Staphylococcus aureus, Mycobacterium tuberculosis*). The alignment is limited to the interface region and numbering is based on the *E. coli* primary sequence. Residues highlighted with different shades of blue indicate different level of conservation (from deep blue: strongly conserved, to white: not conserved). Residues highlighted in brown and orange are involved in surface interactions in the *E. coli* and *T. thermophilus* 43K-COU complexes, respectively. Corresponding secondary structures of the GyrB protein are depicted above the primary sequence.

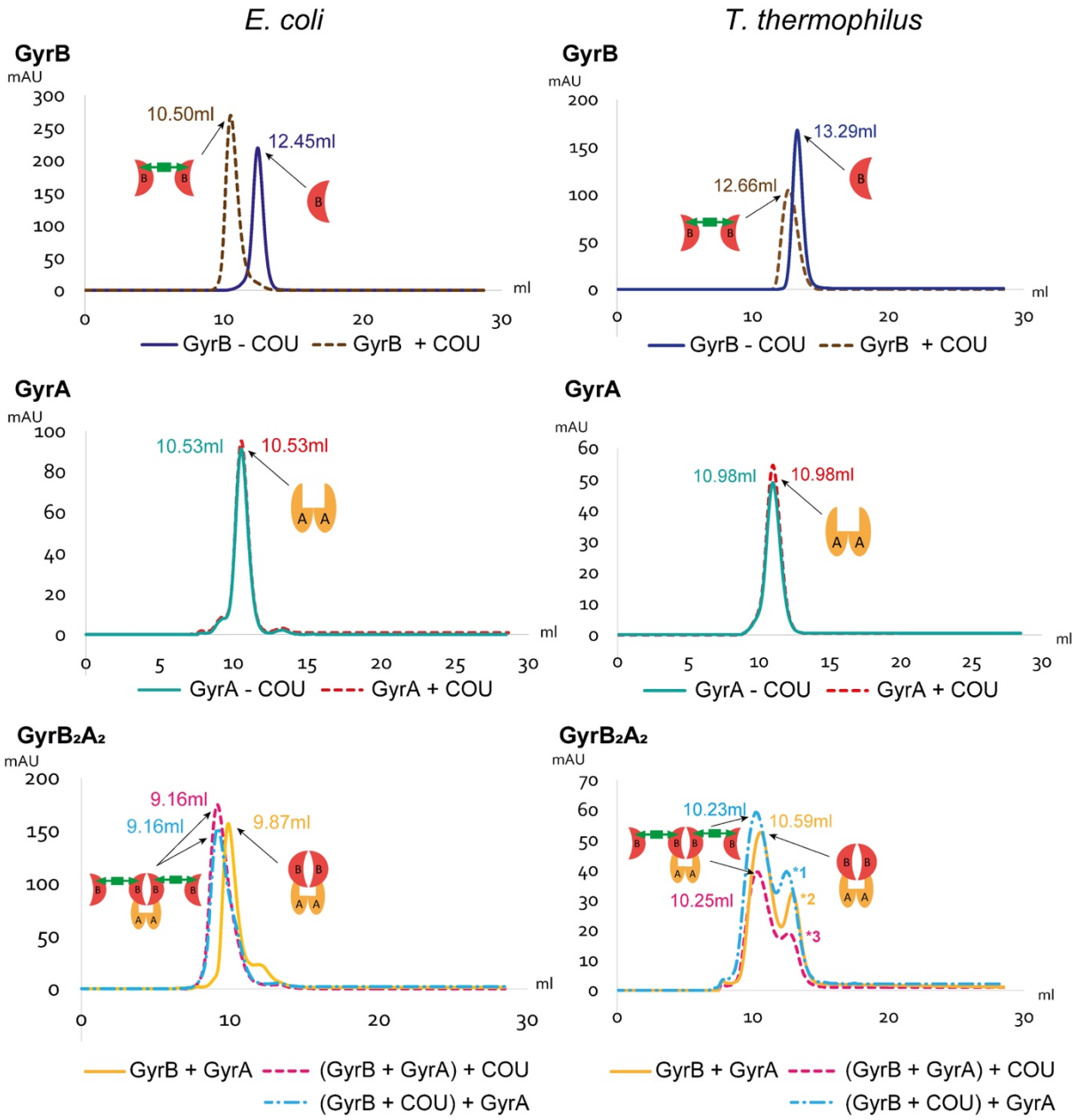

Figure S10. In-solution analysis of GyrB, GyrA and DNA Gyrase in presence of coumermycin A1. Size-exclusion chromatography of *E. coli* (left) and *T. thermophilus* (right) GyrB (top), GyrA (middle) subunits and DNA Gyrase (bottom) alone or in complex with coumermycin A1. In presence of COU, the complete GyrB subunit dimerizes the same way as the GyrB 43K fragment. As expected, no modification of the elution volume of GyrA is observed in presence of COU. The addition of COU to fully reconstituted DNA Gyrase ($GyrB_2A_2$) triggers the formation of a bigger complex which could be attributed to a GyrB-4:2-GyrA stoichiometry ($GyrB_4A_2$). The addition of GyrA subunit to a trapped $GyrB_2$-COU dimer results in the same complex formation ($GyrB_4A_2$). The size-exclusion chromatograms are colored in purple for GyrB in absence of COU, dashed brown for GyrB in presence of COU, cyan for GyrA in absence of COU, dashed red *for* GyrA in presence of COU, yellow for DNA Gyrase (GyrB + GyrA) in absence of COU, dashed pink for DNA Gyrase (GyrB + GyrA) in presence of COU and dashed-dotted blue for GyrB complexed with COU supplemented with GyrA.

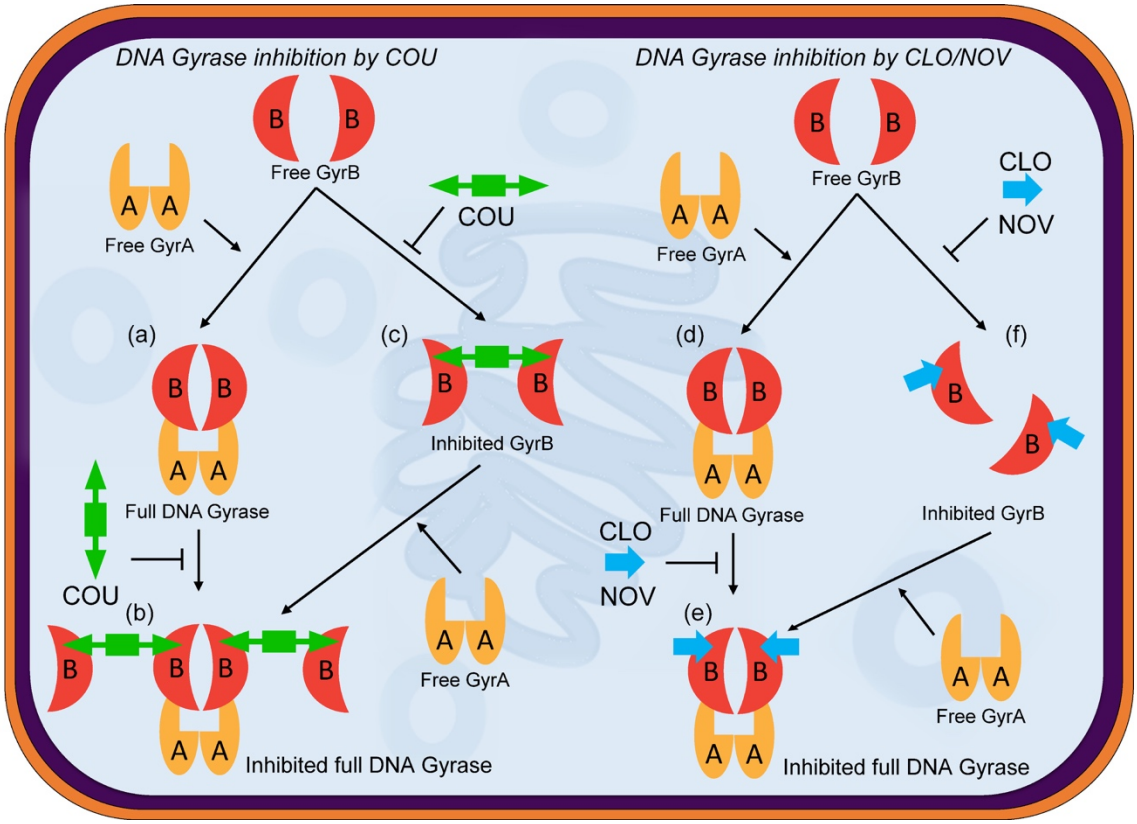

Figure S11. ***In vivo*** **model for the DNA Gyrase inhibition by the aminocoumarins. Left:** proposed mechanism of inhibition of DNA Gyrase by the coumermycin A1 (COU). Once COU has entered the bacteria, it is able to inhibit a fully reconstituted DNA Gyrase complex **(a)** and trap two free GyrB subunits creating a larger complex with 4 GyrB subunits and 2 GyrA subunits ($GyrB_4A_2$) **(b)**. The COU can also sequester free GyrB subunits by creating inhibited dimers **(c)**. Upon GyrA recognition and binding, these trapped dimers may assemble into an inactive $GyrB_4A_2$ **(b)**. **Right:** mechanism of inhibition of DNA Gyrase by novobiocine (NOV) or clorobiocine (CLO). Once NOV or CLO has entered the bacteria, they can inhibit either already formed $GyrB_2A_2$ complexes **(d-e)** or free GyrB subunits **(f)**. Inhibited free GyrB subunits are still able to form a $GyrB_2A_2$ complex with free GyrA subunits **(e)**.

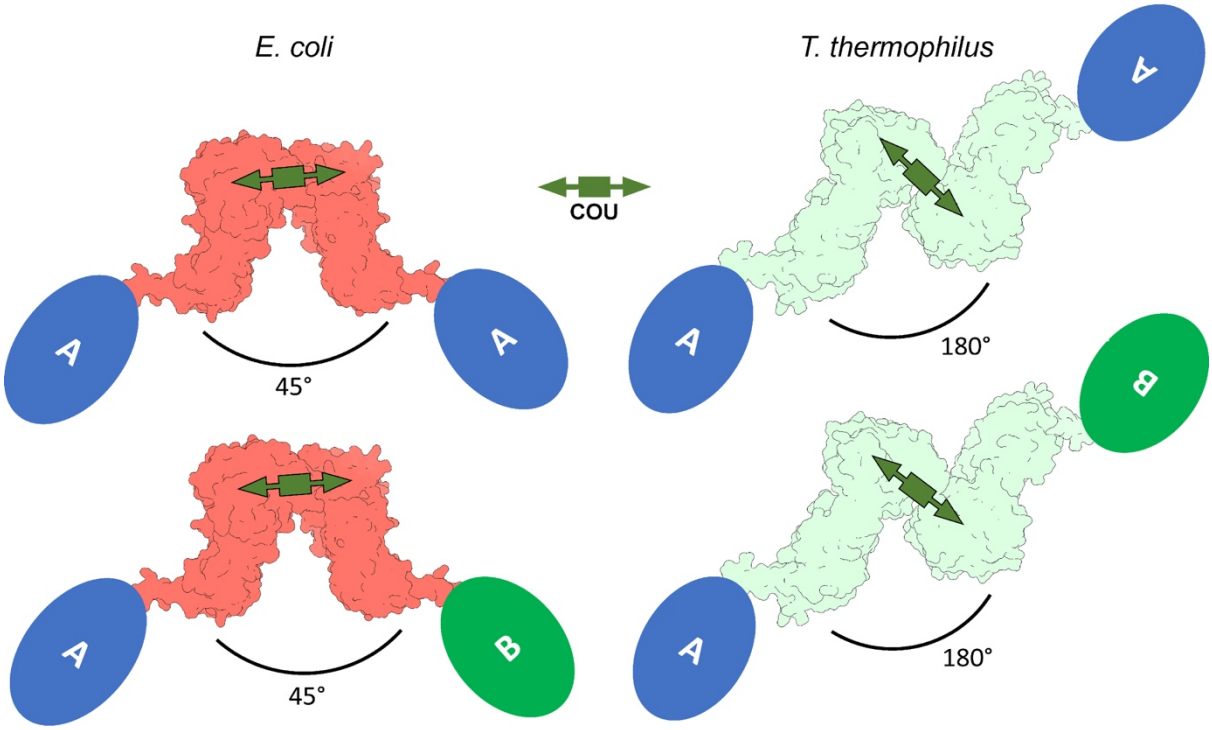

Figure S12. **Chemically-induced dimerization of proteins fused to GyrB**. Fusion of a protein of interest to *E. coli* GyrB 43K (left) and *T. thermophilus* GyrB 43K (right). Upon COU binding, a dimer will be formed forcing the fused protein to dimerize. A 45°-angle between the monomers can be obtained by using the *E. coli* GyrB 43K. A 180°-angle between the monomers can be obtained by using the *T. thermophilus* GyrB 43K. This may be used to dimerize identical or different proteins of interest and induce activities with different geometries.

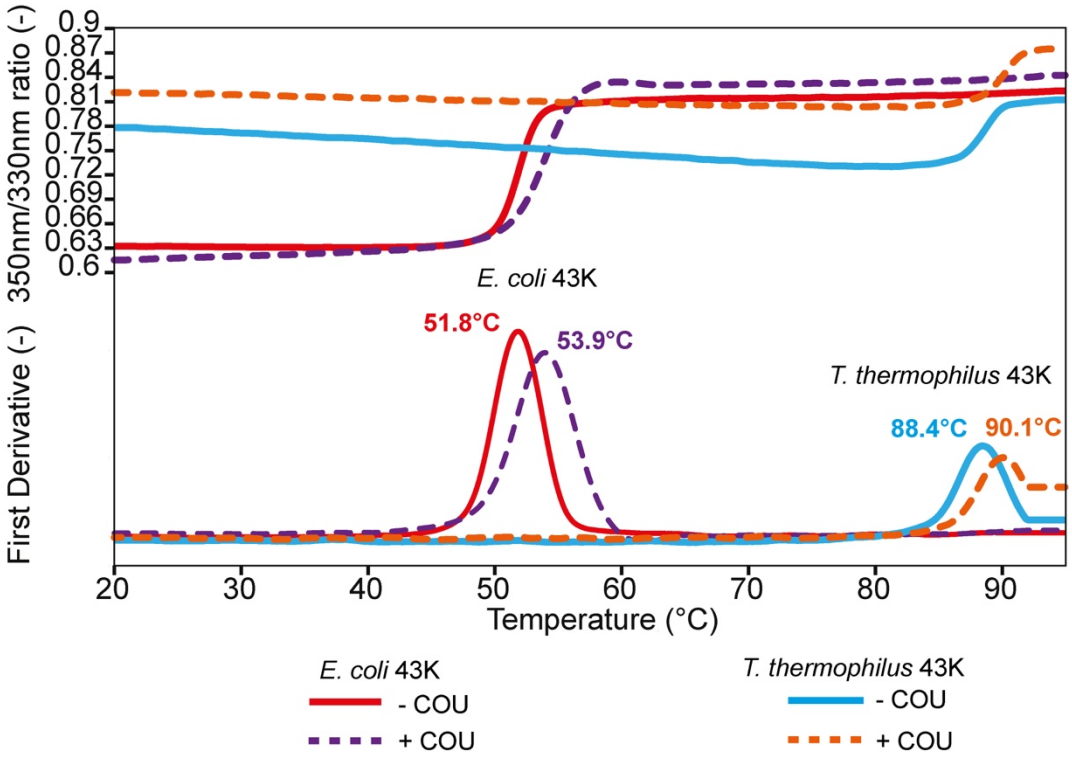

Figure S13. Differential scanning fluorometry analysis. The curves for the *E. coli* 43K monomer are represented in red, the *E. coli* 43K-COU complex in dashed purple, the *T. thermophilus* 43K monomer in blue and *T. thermophilus* 43K-COU complex in dashed orange. First derivative peak corresponds to denaturation mid-point (T_m). Mid-point denaturation temperatures are indicated accordingly.

SUPPLEMENTARY REFERENCES

1. Kabsch, W. Xds. *Acta Crystallogr D Biol Crystallogr* **2010,** 66, 125-132.
2. McCoy, A. J.; Grosse-Kunstleve, R. W.; Adams, P. D.; Winn, M. D.; Storoni, L. C.; Read, R. J. Phaser crystallographic software. *J Appl Crystallogr* **2007,** 40, 658-674.
3. Brino, L.; Urzhumtsev, A.; Mousli, M.; Bronner, C.; Mitschler, A.; Oudet, P.; Moras, D. Dimerization of Escherichia coli DNA-gyrase B provides a structural mechanism for activating the ATPase catalytic center. *J Biol Chem* **2000,** 275, 9468-9475.
4. Lamour, V.; Hoermann, L.; Jeltsch, J. M.; Oudet, P.; Moras, D. An open conformation of the Thermus thermophilus gyrase B ATP-binding domain. *J Biol Chem* **2002,** 277, 18947-18953.
5. Emsley, P.; Lohkamp, B.; Scott, W. G.; Cowtan, K. Features and development of Coot. *Acta Crystallogr D Biol Crystallogr* **2010,** 66, 486-501.
6. Bricogne G., B. E., Brandl M., Flensburg C., Keller P., Paciorek W.,; Roversi P, S. A., Smart O.S., Vonrhein C., Womack T.O. BUSTER 2.10.2. *Cambridge, United Kingdom: Global Phasing Ltd.* **2017**.
7. Goddard, T. D.; Huang, C. C.; Meng, E. C.; Pettersen, E. F.; Couch, G. S.; Morris, J. H.; Ferrin, T. E. UCSF ChimeraX: Meeting modern challenges in visualization and analysis. *Protein Sci* **2018,** 27, 14-25.
8. Konarev, P. V.; Volkov, V. V.; Sokolova, A. V.; Koch, M. H. J.; Svergun, D. I. PRIMUS: a Windows PC-based system for small-angle scattering data analysis. *Journal of Applied Crystallography* **2003,** 36, 1277-1282.
9. Guinier, A., Fournet, G. Small angle scattering of X-rays. *John Wiley and Son, New York* **1955**.
10. Svergun, D. Determination of the regularization parameter in indirect-transform methods using perceptual criteria. *Journal of Applied Crystallography* **1992,** 25, 495-503.
11. Franke, D.; Svergun, D. I. DAMMIF, a program for rapid ab-initio shape determination in small-angle scattering. *Journal of Applied Crystallography* **2009,** 42, 342-346.
12. M. J. Frisch, G. W. T., H. B. Schlegel, G. E. Scuseria, M. A. Robb, J. R. Cheeseman, G. Scalmani, V. Barone, G. A. Petersson, H. Nakatsuji, X. Li, M. Caricato, A. Marenich, J. Bloino, B. G. Janesko, R. Gomperts, B. Mennucci, H. P. Hratchian, J. V. Ortiz, A. F. Izmaylov, J. L. Sonnenberg, D. Williams-Young, F. Ding, F. Lipparini, F. Egidi, J. Goings, B. Peng, A. Petrone, T. Henderson, D. Ranasinghe, V. G. Zakrzewski, J. Gao, N. Rega, G. Zheng, W. Liang, M. Hada, M. Ehara, K. Toyota, R. Fukuda, J. Hasegawa, M. Ishida, T. Nakajima, Y. Honda, O. Kitao, H. Nakai, T. Vreven, K. Throssell, J. A. Montgomery, Jr., J. E. Peralta, F. Ogliaro, M. Bearpark, J. J. Heyd, E. Brothers, K. N. Kudin, V. N. Staroverov, T. Keith, R. Kobayashi, J. Normand, K. Raghavachari, A. Rendell, J. C. Burant, S. S. Iyengar, J. Tomasi, M. Cossi, J. M. Millam, M. Klene, C. Adamo, R. Cammi, J. W. Ochterski, R. L. Martin, K. Morokuma, O. Farkas, J. B. Foresman, D. J. Fox. Gaussian 09. *Gaussian, Inc., Wallingford CT* **2016**.
13. Krissinel, E.; Henrick, K. Inference of macromolecular assemblies from crystalline state. *J Mol Biol* **2007,** 372, 774-797.
14. Adams, P. D.; Afonine, P. V.; Bunkoczi, G.; Chen, V. B.; Davis, I. W.; Echols, N.; Headd, J. J.; Hung, L. W.; Kapral, G. J.; Grosse-Kunstleve, R. W.; McCoy, A. J.; Moriarty, N. W.; Oeffner, R.; Read, R. J.; Richardson, D. C.; Richardson, J. S.; Terwilliger, T. C.; Zwart, P. H. PHENIX: a comprehensive Python-based system for macromolecular structure solution. *Acta Crystallogr D Biol Crystallogr* **2010,** 66, 213-221.
15. Karplus, P. A.; Diederichs, K. Linking crystallographic model and data quality. *Science* **2012,** 336, 1030-1033.
16. Brunger, A. T. Free R value: a novel statistical quantity for assessing the accuracy of crystal structures. *Nature* **1992,** 355, 472-475.
17. Svergun, D.; Barberato, C.; Koch, M. H. J. CRYSOL - a Program to Evaluate X-ray Solution Scattering of Biological Macromolecules from Atomic Coordinates. *Journal of Applied Crystallography* **1995,** 28, 768-773.
18. Petoukhov, M. V.; Svergun, D. I. Global rigid body modeling of macromolecular complexes against small-angle scattering data. *Biophys J* **2005,** 89, 1237-1250.